



Manipulating density of magnetic skyrmions via multilayer repetition and thermal annealingXinran Wang,^{1,2} Anni Cao,^{1,4} Sai Li,¹ Jin Tang,³ Ao Du,¹ Houyi Cheng,¹ Yiming Sun ¹,
Haifeng Du,³ Xueying Zhang,^{1,2,*} and Weisheng Zhao ^{1,2,†}¹*Fert Beijing Institute, School of Integrated Circuit Science and Engineering,
Beijing Advanced Innovation Center for Big Data and Brain Computing,
Beihang University, Beijing 100191, China*²*Beihang-Goertek Joint Microelectronics Institute, Qingdao Research Institute,
Beihang University, Qingdao 266000, China*³*Anhui Province Key Laboratory of Condensed Matter Physics at Extreme Conditions,
High Magnetic Field Laboratory of Chinese Academy of Sciences,
and University of Science and Technology of China, Hefei 230031, China*⁴*Beijing Microelectronics Technology Institute, Beijing 100076, China*

(Received 16 June 2021; revised 23 July 2021; accepted 26 July 2021; published 11 August 2021)

The magnetic skyrmion, a tiny magnetic texture that holds promise as the next-generation information carrier, has been widely studied in recent years. A fine tunability of skyrmion density is required for its real applications in novel memory and logic devices. Here, we report on the manipulation of skyrmion density at room temperature in a Pt/Co/Ta/MgO system composed of multiple repetitions with perpendicular magnetic anisotropy. Néel-type skyrmions are observed by performing Lorentz transmission electron microscopy and magnetic force microscopy. The influence of structure repetition on skyrmions is experimentally investigated and further understood by micromagnetic simulations. The variation of skyrmion density with repetition number is mainly attributed to magnetic anisotropy. Meanwhile, thermal annealing is utilized to regulate the skyrmion density, where skyrmion-related properties exert a competitive effect. Our findings provide alternative means to manipulate skyrmion density, further allowing for optimized engineering of skyrmion-based devices.

DOI: [10.1103/PhysRevB.104.064421](https://doi.org/10.1103/PhysRevB.104.064421)**I. INTRODUCTION**

The magnetic skyrmion [1,2], a topological magnetic texture, is of particular interest since it is expected to be the next generation of information carriers [3,4]. Due to their small size, topological protection, and efficient current-driving dynamics [5,6], skyrmions are promising as applications in novel electronic devices, such as racetrack memory [7] and neuromorphic computing devices [8–11]. Skyrmions were first observed in B20-type bulk material MnSi [1] and then found in epitaxial magnetic films composed of Fe or PdFe monolayers on Ir (111) [12,13]. However, the narrow temperature zone and strict fabrication technology for such material systems hinder the related application and integration.

Recently, the multiply repetitive heavy metal (HM)/ferromagnetic (FM) multilayers hosting skyrmions deposited by magnetron sputtering have attracted tremendous attention. A relatively large Dzyaloshinskii-Moriya Interaction (DMI) can be induced at the HM/FM interface due to the strong spin-orbit coupling (SOC) of the HM layers [14–16], which is essential for stabilizing chiral spin texture such as skyrmions. The increasing effective magnetic thickness enables the stability of skyrmions at room temperature [17]. In addition, one

advantage of the multirepeated multilayer structure is that the properties of skyrmions can be fine tuned [18–22]. Skyrmions in such structures can be controlled through the competition among different items like DMI, magnetic anisotropy, dipole-dipole interaction, and exchange interaction [23]. For example, skyrmion density in [Pt/Co/Ta]_N has been elaborately modulated by changing the Co thickness [20], and the crossover from a few isolated skyrmions to a dense skyrmion lattice has been realized by adjusting the Co and Fe composition in [Ir/Fe/Co/Pt]_N [18]. However, concerning the structure repetition number, the variation of skyrmion density has not been systematically explored and the physical mechanism needs to be revealed. Several works have investigated the variations of twist domain walls or other magnetic parameters [24–26] with different structure repetition numbers, while research focused on skyrmions is still needed.

On the other hand, the electrical detection by magnetoresistance (MR) is the core issue for practical applications of skyrmions [27]. In order to enhance the MR, thermal annealing is widely used in the semiconductor process to produce a crystallized MgO tunnel barrier [28,29]. Previous works [30–32] have focused on the correlation between thermal annealing and magnetic intrinsic properties such as DMI and magnetic anisotropy. These magnetic properties have been demonstrated to have direct implications for skyrmions [18,33,34]; therefore it is desirable to check the influence of the annealing process on the properties of

*xueying.zhang@buaa.edu.cn

†weisheng.zhao@buaa.edu.cn

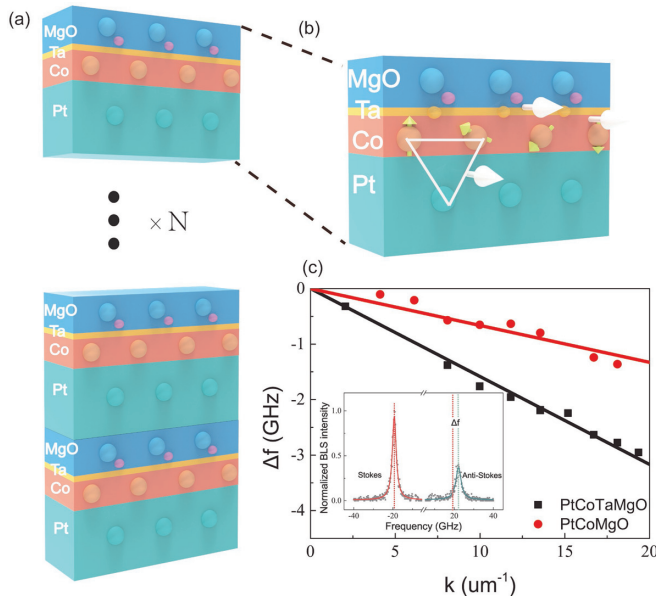


FIG. 1. (a) Schematic of the sample structure, featuring different repeat numbers of Pt/Co/Ta/MgO multilayers. (b) Detailed schematic of the Pt/Co/Ta/MgO multilayer stack, exhibiting corresponding interfacial DMI. (c) The linear dependence of Δf on k obtained by BLS measurements to quantify DMI constant of Pt/Co/MgO samples, and the inset shows typical BLS spectra for $k = 21.40 \mu\text{m}^{-1}$ where the spin wave propagation is the DE mode.

skyrmions in a more direct way, and further to develop an efficient method to tune the skyrmion density.

Our previous work found that the interfacial quality and DMI could be enhanced significantly [32,35] by inserting a Ta layer at the Co/MgO interface in the Pt/Co/MgO system, which is an optimized material platform to host skyrmions at room temperature. In this paper, the remarkable enhancement of DMI is verified by performing Brillouin light scattering (BLS) measurements. We engineer the $[\text{Pt}/\text{Co}/\text{Ta}/\text{MgO}]_N$ multirepeated multilayers stack with perpendicular anisotropy; the existence of Néel-type skyrmions is confirmed by Lorentz transmission microscopy (LTEM). Then we investigate how the variation of repeating number N influences skyrmion density in experiments and in simulations. In addition, the thermal annealing process is used to adjust magnetic properties such as DMI and perpendicular magnetic anisotropy (PMA), and the relationship between annealing temperature and skyrmion density η_{sk} is unveiled. Our research provides feasible approaches to tune skyrmion density, paving the way toward skyrmion-based spintronic devices.

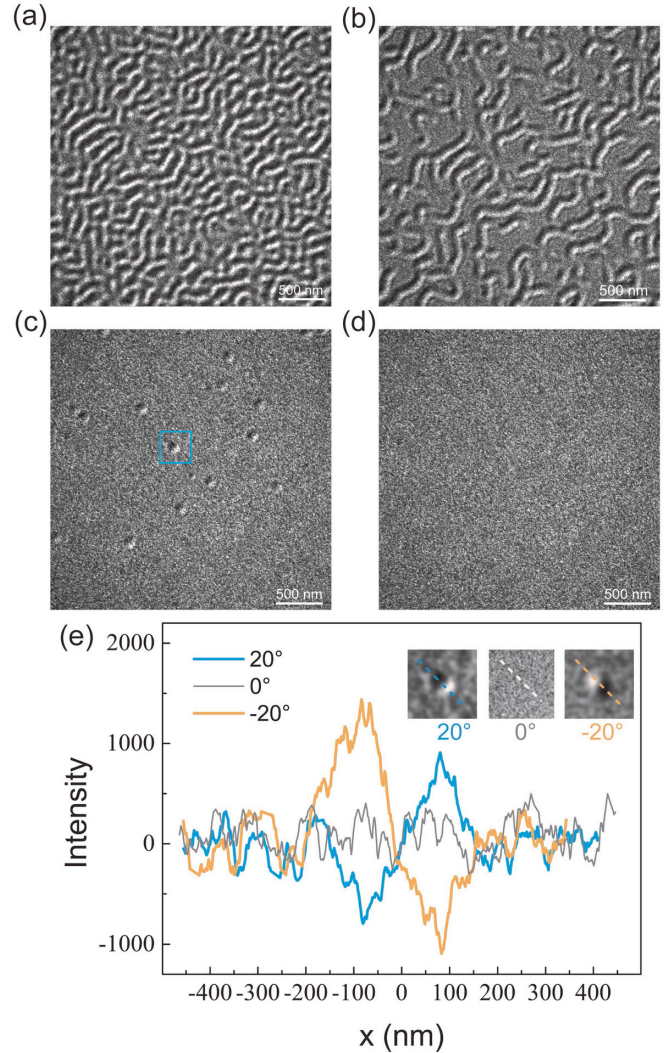


FIG. 2. LTEM images obtained in 20° tilting condition and defocus mode, and under different perpendicular magnetic fields (a) for $\mu_0 H = 0 \text{ mT}$, (b) for $\mu_0 H = 46 \text{ mT}$, (c) for $\mu_0 H = 63 \text{ mT}$, and (d) for $\mu_0 H = 74 \text{ mT}$. (e) Line profiles of magnetic skyrmions (insets) extracted from LTEM images with tilting angles $+20^\circ$, 0° , and -20° .

II. SAMPLE PREPARATION

$\text{Ta}(3\text{nm})/[\text{Pt}(4\text{nm})/\text{Co}(1.7\text{nm})/\text{Ta}(0.2\text{nm})/\text{MgO}(2\text{nm})]_N/\text{Pt}(5\text{ nm})$ samples were grown by using magnetron sputtering at room temperature and a basic pressure around $3 \times 10^{-8} \text{ mbar}$. As shown in Fig. 1(a), N represents repeat numbers varying from 1 to 10 and the detailed structure of each repeated layer is shown in Fig. 1(b). The substrates used

TABLE I. Results of BLS measurements to quantify DMI constant D for different samples.

Sample	$\gamma/2\pi$ [41] (GHz/T)	Slope of $\Delta f/k$ (GHz/ μm)	M_s ($\times 10^5 \text{ A/m}$)	D (mJ/m^2)
Pt/Co/MgO	30.55	0.070 ± 0.004	11.4 ± 1.35	0.66 ± 0.12
Pt/Co/Ta/MgO	30.55	0.155 ± 0.003	8.98 ± 0.45	1.15 ± 0.07
$[\text{Pt}/\text{Co}/\text{Ta}/\text{MgO}]_5$	30.55	0.142 ± 0.003	9.76 ± 0.93	1.14 ± 0.13
$[\text{Pt}/\text{Co}/\text{Ta}/\text{MgO}]_{10}$	30.55	0.144 ± 0.002	9.45 ± 0.86	1.12 ± 0.09

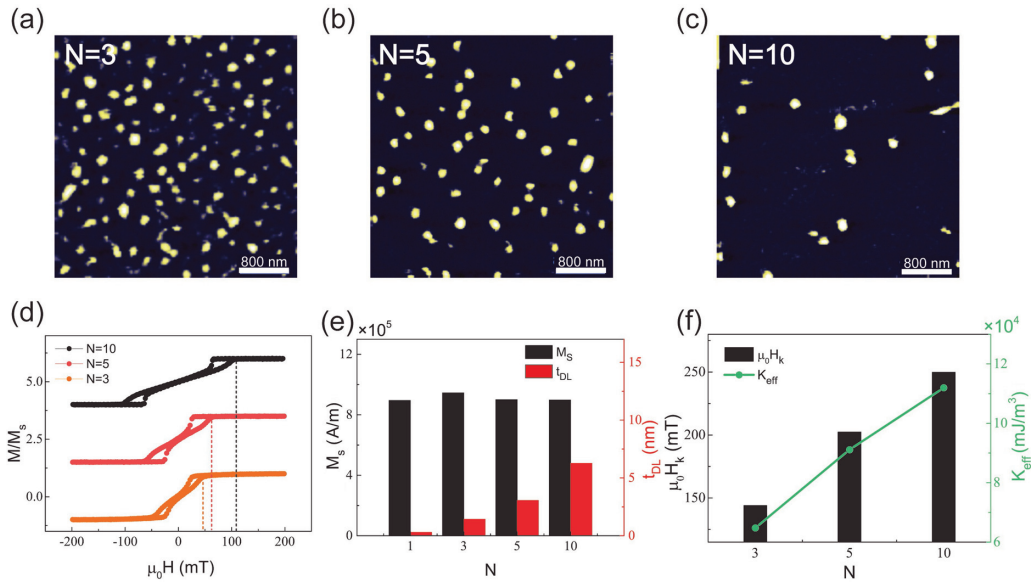


FIG. 3. (a–c) Room-temperature MFM images corresponding to the state with maximum skyrmion density for $[\text{Pt}/\text{Co}/\text{Ta}/\text{MgO}]_N$ samples under a magnetic field of $\mu_0 H = 29$ mT, $\mu_0 H = 58$ mT, $\mu_0 H = 89$ mT respectively. (d) Normalized perpendicular hysteresis loops of Pt/Co/Ta/MgO samples of different N measured by VSM. The loops are shifted vertically for clarity. The dashed lines indicate the saturated field. (e,f) Magnetic properties including M_s , H_k , t_{BL} , and K_{eff} obtained from the hysteresis loops for different N .

are silicon plates with 100-nm thermal silicon oxide layers, while the Lorentz TEM specimen is grown on a 50 nm thick (Si_3N_4) membrane. The bottom Ta buffer layer is used to improve the interfacial quality of Pt/Co/MgO layers [36]. The top Pt layer prevents the film from air passivation. A dusting Ta layer is inserted between Co and MgO to prevent the deterioration of the Co/MgO interface during the deposition process, and improve the crystallization for both ferromagnetic and insulating layers [32].

III. RESULTS AND DISCUSSIONS

The interfacial DMI is defined by neighboring spins [5,37]: $\mathcal{H}_{\text{DMI}} = \vec{D}_{i,j} \cdot (\vec{S}_i \times \vec{S}_j)$, where $\vec{D}_{i,j}$ is a DMI vector and \vec{S}_i and \vec{S}_j are two neighboring spins. As calculated in our previous report, such structure exhibits strong DMI due to the contributions from both the Pt/Co and Co/MgO interface [32]. The strength of the DMI of our samples is quantified by BLS measurements, which detect the asymmetric dispersion of spin waves induced by DMI [38,39]. The measurements are performed in the Damon-Eshbach (DE) mode where an in-plane magnetic field is applied. A green laser beam is focused on the sample surface using an objective as the incident light, and the backscattered lights are collected and sent to a six-pass tandem Fabry-Perot interferometer. BLS spectra are obtained after the accumulation of photons for several hours to improve the signal to noise ratio, as presented in the inset of Fig 1(c); the Stokes and anti-Stokes peaks of the spectrum are determined assisted by Lorenz function fitting. Thus, the frequency difference of the counterpropagating spin waves $\Delta f = f_s - f_{as}$ reveals the presence of DMI. According to the following equation [40]— $\Delta f = 2\gamma Dk/\pi M_s$, where γ is the gyromagnetic ratio, M_s is the saturated magnetization which can be measured by vibrating sample magnetometry

(VSM), and k is the amplitude of the wave vector—the DMI constant D could be extracted from the linear fittings of the Δf – k scatterplot, as shown in Fig. 1(c). The magnetic parameters used and the determined D of the Pt/Co/MgO and Pt/Co/Ta/MgO samples are summarized in Table I, as 0.66 ± 0.12 and 1.15 ± 0.07 mJ/m², respectively. A noticeable enhancement of DMI value with the inserted Ta layer is found, in agreement with our previous report, meaning that these structures could host skyrmions.

Pt/Co/Ta/MgO with multiple repetitions studied here possess perpendicular magnetic anisotropy (PMA), while the perpendicular hysteresis loops exhibit typical sheared shapes (see Supplemental Material [42]; also see [43]). Here we perform Lorentz transmission electron microscopy (LTEM, Talos F200X) measurements to observe the skyrmions phase in six-repetition $[\text{Pt}/\text{Co}/\text{Ta}/\text{MgO}]_6$ multilayers. The measurements are carried out at room temperature, in the defocus mode of 7.9 mm, and with a $+20^\circ$ tilt of the sample normal with respect to the beam axis. The external magnetic field is applied parallel to the electron beam. Figures 2(a)–2(d) depict the evolution of domain states from the labyrinth domain at zero field, gradually to the isolated skyrmions phase under a certain field, and finally reach the saturated state with the increasing external perpendicular magnetic field. The domain structures are determined by the competition between DMI, dipole-dipole interaction, magnetic anisotropy, and exchange interaction, where the large interfacial DMI facilitates the formation and stabilization of Néel-type domain walls and skyrmions. To confirm the Néel configuration of skyrmions in this structure, we extract the magnified images of a single skyrmion [the one in the blue box of Fig. 2(c)] by taking a tilt series of -20° , 0° , and $+20^\circ$, as shown in the inset of Fig. 2(e). Without tilting, no image contrast can be seen, while with opposite tilt angles, the dark-bright image contrast

is reversed. These imaging features confirm the existence of stable Néel skyrmions in Pt/Co/Ta/MgO structures [44–46]. The corresponding line profile with a cut width of 21 nm is shown in Fig. 2(e), which shows that the skyrmion size is $154 \text{ nm} \pm 12 \text{ nm}$.

Notably, we find that the skyrmion density varies with numbers of repetition N . It has been reported that the applied in-plane component of the magnetic field introduced by the necessary tilt angle of LTEM measurements will affect the concentration of skyrmions [44]. Thus, magnetic force microscopy (MFM, Bruker Icon system) is used [47] to investigate the dependence of skyrmion density η_{sk} on N . Low-moment magnetic probes (Nanosensors PPP-LM) are used. The evolution of domain states for these samples is quite similar and in agreement with LTEM images (see Supplemental Material [42]). They all exhibit the maze domain state at lower field; with the increasing magnetic field, the domains gradually shrink and the isolated skyrmions appear. Figures 3(a)–3(c) show the room temperature MFM images corresponding to the state with maximum skyrmion density η_{sk} for each sample under a certain magnetic field of $\mu_0 H = 29 \text{ mT}$, $\mu_0 H = 58 \text{ mT}$, $\mu_0 H = 89 \text{ mT}$ respectively. We can see that for different N , the number of isolated skyrmions that appeared is decreasing with the increase of N .

To explore the physical mechanism of N -dependent skyrmion density, the change of several magnetic properties with repeat number N is probed. The normalized perpendicular and in-plane hysteresis loops of $[\text{Pt}/\text{Co}/\text{Ta}/\text{MgO}]_N$ samples are shown in the Supplemental Material [42]. All perpendicular loops exhibit a sheared shape, while the saturation field and the applied field required to reach the skyrmion state increase with N , which is mainly caused by the increasing dipolar interaction [23]. The saturated magnetization M_s and dead layer thickness t_{DL} can be obtained from M/A vs t_{Co} curves [43], where M is the magnetization extracted from the perpendicular hysteresis loops, a is the sample area, and t_{Co} is the thickness of Co [42]. As can be seen in Fig. 3(e), the saturated magnetization M_s remains almost stable in the N range studied, while t_{DL} increases proportionally to N , indicating an average t_{DL} about 0.5–0.7 nm for each Pt/Co/Ta/MgO repetition. The magnetic perpendicular anisotropy can be evaluated by $K_{\text{eff}} = \mu_0 M_s H_k / 2$, where $\mu_0 H_k$ is the effective anisotropy field extracted from the in-plane hysteresis loops [48]. The dependence of K_{eff} on the repetition number N is plotted in Fig. 3(f). We find a considerable rise of K_{eff} from 6.48×10^4 to $1.12 \times 10^5 \text{ J/m}^3$ with the increasing N , which may attribute to the elastic strain induced by magnetoelastic interface anisotropy [25,49,50]. Moreover, by BLS measurements, we find the D value of $[\text{Pt}/\text{Co}/\text{Ta}/\text{MgO}]_N$ is comparable with that of nonrepeated Pt/Co/Ta/MgO multilayers, as shown in Table I. Thus we verify that the constant D is substantially not sensitive to the repetition number N [47,51]. This result indicates that the DMI strength for multilayers composed of multiple repetitions can be regarded the same as that of individual layers. However, the change of effective perpendicular anisotropy is non-negligible.

The dependence of K_{eff} and maximum η_{sk} on repetition number N is shown in Fig. 4(a), where negative correlation existing between η_{sk} and K_{eff} can be found. It implies that stronger effective perpendicular anisotropy is unfavorable for

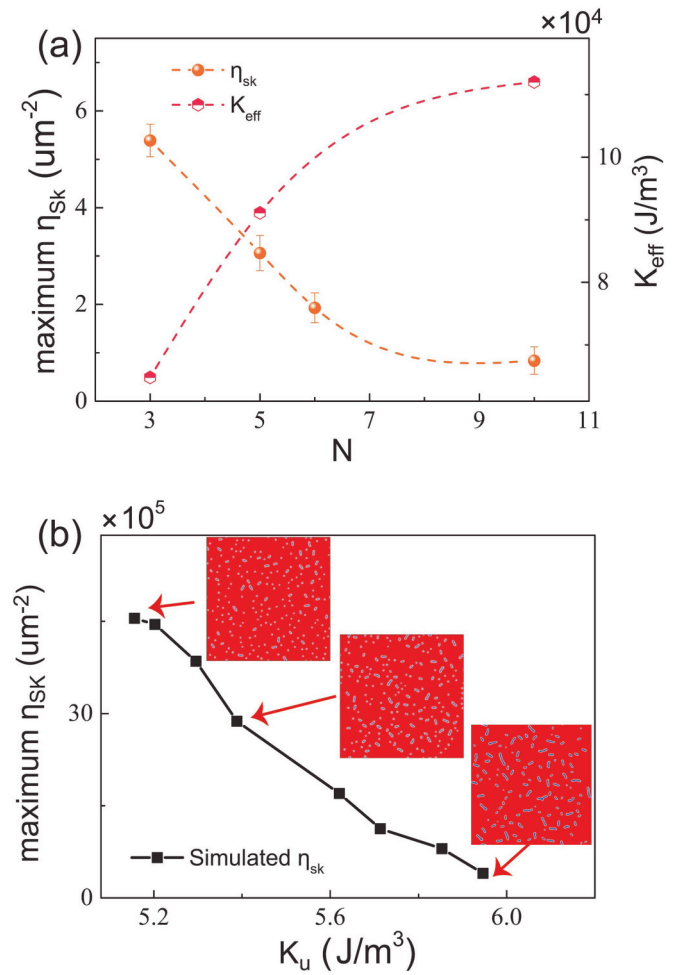


FIG. 4. (a) Experimentally measured skyrmion density η_{sk} and variation of K_{eff} with repetition number N . (b) Simulated skyrmion density η_{sk} variation with K_u .

the skyrmion formation, which may be the major reason for the dependence of skyrmion density on repetition number N in the studied multilayer. To gain more insight, micromagnetic simulations are carried out with the MUMAX3 software package [52]. As discussed earlier by Woo *et al.* [53], the whole multirepeated multilayer stack can be modeled as a single magnetic layer using an effective scaling law, so the simulations are performed using the approach proposed with a cell size of $4 \times 4 \text{ nm}^2$ ($x \times y$) in an area of $2 \times 2 \text{ um}^2$. More details of micromagnetic simulations including scaling laws can be found in the Supplemental Material [42]. Considering the saturated magnetization M_s remains almost unchanged for different repeat numbers, we take an average value of $0.9 \times 10^6 \text{ A/m}$, with exchange constant A of $1.0 \times 10^{-11} \text{ J/m}$ and DMI energy of 1.2 mJ/m^2 . The evolution of the magnetic domain is observed in the simulation when the uniaxial anisotropy $K_u = K_{\text{eff}} + \mu_0 M_s^2 / 2$ with $K_{\text{eff}} > 0$ varies. The experimental observation of maze domain–stripe–isolated skyrmions state transition with the external magnetic field is qualitatively reproduced by simulations [42]. With the increasing K_u , the maximum skyrmion density exhibits a decreasing trend shown in Fig. 4(b). The insets of Fig. 4(b) show the simulated images corresponding the state with maxi-

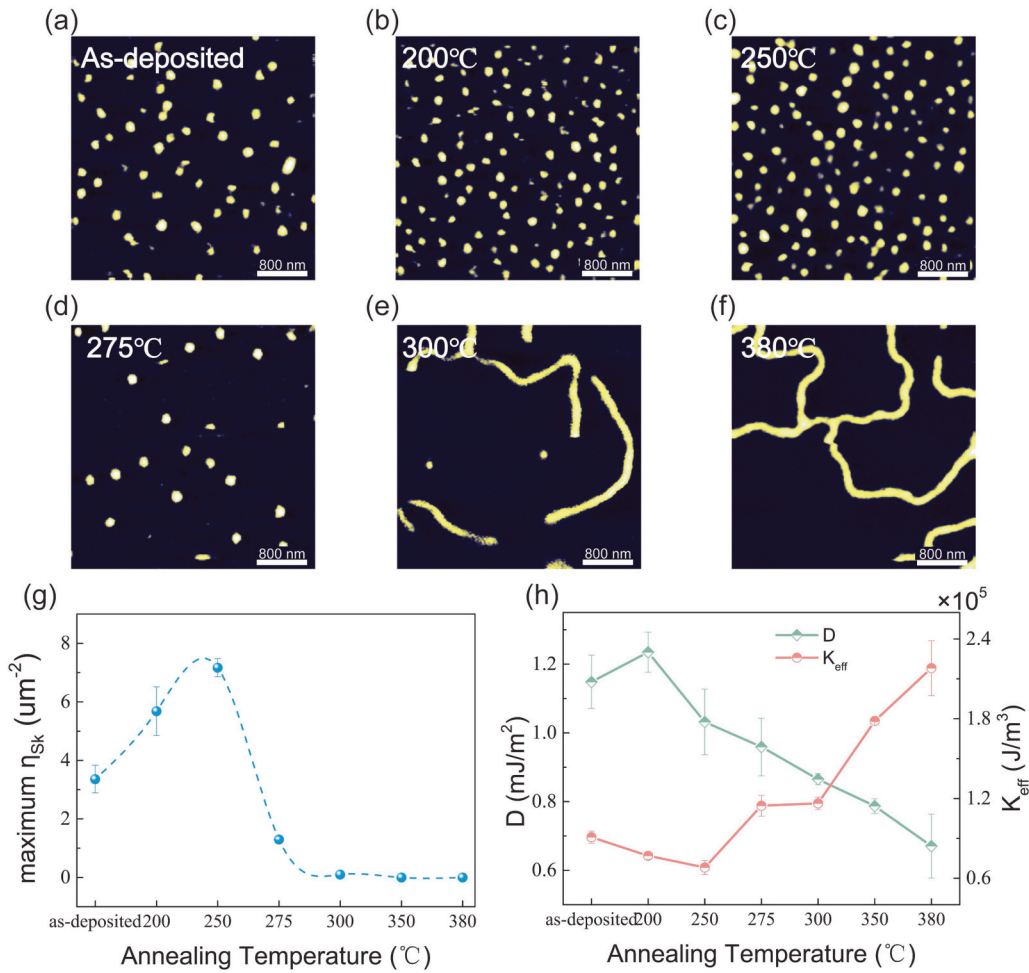


FIG. 5. (a)–(f) Room-temperature MFM images corresponding to the state with maximum skyrmion density of [Pt/Co/Ta/MgO]₅ samples annealed at different temperatures. (g) Variation of skyrmion density η_{sk} as a function of annealing temperature. (h) Variation of DMI constant D and perpendicular anisotropy K_{eff} as a function of annealing temperature.

imum η_{sk} . The consistency between simulation and experiment suggests that N -dependent changes in K_{eff} mainly contribute to the variation behaviors of η_{sk} .

As our previous work unveiled a relationship between thermal annealing temperature and DMI in similar structure [32], the role of thermal annealing on manipulating skyrmions is worth exploring further. Based on our above investigation of skyrmion observation in [Pt/Co/Ta/MgO]_N structures, samples of $N = 5$ with moderate skyrmion density are chosen to be annealed for a half hour at temperatures ranging from 200°C to 380°C. The duration of temperature rising is 30 min, with a 500-mT applied perpendicular field when annealing.

The magnetic state with maximum density of isolated skyrmions under a certain magnetic field is observed using MFM, as shown in Figs. 5(a)–5(f). For annealing temperature higher than 350°C, the transition of stripe domains to skyrmions cannot be observed. The dependence of η_{sk} on annealing temperature is present in Fig. 5(g), exhibiting a trend of increase followed by a decrease. The η_{sk} reaches an optimal value about $7.17 \pm 0.31 \mu\text{m}^{-2}$ after an annealing process at around 250°C, which is almost 2–3

times improvement compared with the as-deposited sample, while beyond this temperature, η_{sk} decreases continuously, even down to zero when higher than 350°C. It indicates the annealing is an effective tool to alter skyrmion density.

To further understand the possible reasons for the η_{sk} dependence on annealing temperature, we focus on the DMI and anisotropy variation, which have been proved to be the key parameters affecting the properties of skyrmions [18,20]. The basic magnetic properties such as M_s , t_{DL} , K_{eff} , and D are extracted from perpendicular and in-plane hysteresis loops as well as the BLS measurements [42]. As we find that M_s and D remain almost unchanged for multiple-repeated sample vs nonrepeated Pt/Co/Ta/MgO structure; therefore, we adopt the measured M_s and D values of the nonrepeated sample to estimate the role of annealing temperature for a five-repetition sample. The saturated magnetization shows weak correlation with annealing temperatures, while the dead layer decreases for temperature higher than 250°C [42], which is consistent with previous studies [43].

Next, we find that D is enhanced up to $1.23 \pm 0.05 \text{ mJ/m}^2$ at 200°C yet monotonously reduced for higher annealing

temperatures. The enhancement of DMI at relatively low annealing temperature could be attributed to the more homogenized oxide layer, which is confirmed by a TEM image [32] and an improved ordering of the atoms at the Pt/Co interface [54], whereas it has been reported [14] that higher annealing temperatures leads to interfacial diffusion, which is detrimental for the DMI [31]. Furthermore, we observe the effective anisotropy field $\mu_0 H_k$ first drops at the early stage and then increases by around 2–3 times with the increase of temperature [42]. As shown in Fig. 5(h), over the investigated temperature range, K_{eff} starts to improve when the temperature reaches 275°C, and the largest improvement appears when the temperature increases higher than 300°C. We speculate that this nonmonotonic variation may be caused by the alternating dominance of the contribution of Pt/Co and Co/MgO interfaces to PMA. It is reported that after the annealing process, the interpenetrated oxygen atoms that diffused to the Co/MgO interface would result in an improved Co/MgO interface, hence a stronger PMA [30,33,55]; in contrast, the intermixing of Pt and Co atoms would cause a decrease in PMA [30]. The role of the inserted layer Ta is mainly to weaken the oxidation of the Co layer during the sputtering process, as confirmed by our previous work [35]. Since it is only 0.2 nm, we could assume that its effect is relatively weak for the interface intermixing and atomic migration caused by annealing.

In general, DMI and K_{eff} exert competitive effects on the regulation of skyrmion densities [18,20,30]. DMI favors non-collinear spin arrangement, favoring the stabilization chiral skyrmions [2], while a moderate reduction of K_{eff} is beneficial for the stability and density increase of skyrmions [20]. This competitive effect can also be described via a material parameter [18] defined as $\kappa = (4/\pi)D/\sqrt{A \cdot K_{\text{eff}}}$ [18], which is positively correlated to skyrmion stability. A larger DMI or lower K_{eff} will contribute to a higher κ . Below an annealing temperature of 200°C, the decrement of K_{eff} and the enhancement of DMI both contribute synergistically to the stability of skyrmions, thus leading to the increase of η_{sk} . At 250°C, despite the slight decline of D , the K_{eff} decreases more, lead-

ing to the further increase of skyrmion density. In this case, DMI and K_{eff} play competitive regulation on the formation of skyrmions. However, when the annealing temperature further increases, both the significant decrease of D and enhancement of PMA are induced, leading to the decrease of skyrmion density. As can be seen from the above experiments, the skyrmion density can be effectively regulated by the annealing process through the modification of DMI and K_{eff} . This result allows for the precise engineering of the skyrmion properties and density, and the optimization of skyrmion-hosting devices.

IV. CONCLUSION

In conclusion, the properties of skyrmion Pt/Co/Ta/MgO multirepetition structures have been systematically studied. Experimental and simulated results indicate the influence of repeat numbers on the skyrmion density η_{sk} could be mainly attributed to K_{eff} . Furthermore, it is found that DMI and PMA can both be tuned simultaneously via the thermal annealing process, leading to the variation of η_{sk} under the competitive effect of these two parameters. At a proper temperature, skyrmion density can be enhanced 2–3 times compared with as-deposited samples, whereas higher temperature will be detrimental for the formation of skyrmions. This study provides alternative means to manipulate the properties and density of skyrmions in multilayers, and highlights the possibility to design high-density skyrmionic devices.

ACKNOWLEDGMENTS

The authors would like to acknowledge the support from the projects from National Natural Science Foundation of China (Grants 61627813 and 61571023), the Beijing Municipal Science and Technology Project under Grant Z201100004220002, the National Key Technology Program of China Grant 2017ZX01032101, the Program of Introducing Talents of Discipline to Universities in China (Grant B16001), the VR innovation platform from Qingdao Science and Technology Commission, and the China Scholarship Council.

-
- [1] S. Mühlbauer, B. Binz, F. Jonietz, C. Pfleiderer, A. Rosch, A. Neubauer, R. Georgii, and P. Böni, *Science* **323**, 915 (2009).
 - [2] U. K. Röbner, A. N. Bogdanov, and C. Pfleiderer, *Nature* **442**, 797 (2006).
 - [3] A. Fert, V. Cros, and J. Sampaio, *Nat. Nanotechnol.* **8**, 152 (2013).
 - [4] W. Kang, Y. Huang, X. Zhang, Y. Zhou, and W. Zhao, *Proc. IEEE* **104**, 2040 (2016).
 - [5] A. Fert, N. Reyren, and V. Cros, *Nat. Rev. Mater.* **2**, 17031 (2017).
 - [6] J. Zhu, Y. D. Wu, Q. Y. Hu, L. Y. Kong, J. Tang, M. L. Tian, and H. F. Du, *Sci. China: Phys., Mech. Astron.* **64**, 227511 (2021).
 - [7] J. Sampaio, V. Cros, S. Rohart, A. Thiaville, and A. Fert, *Nat. Nanotechnol.* **8**, 839 (2013).
 - [8] D. Prychynenko, M. Sitte, K. Litzius, B. Krüger, G. Bourianoff, M. Kläui, J. Sinova, and K. Everschor-Sitte, *Phys. Rev. Appl.* **9**, 014034 (2018).
 - [9] J. Zázvorka, F. Jakobs, D. Heinze, N. Keil, S. Kromin, S. Jaiswal, K. Litzius, G. Jakob, P. Virnau, D. Pinna, K. Everschor-Sitte, L. Rózsa, A. Donges, U. Nowak, and M. Kläui, *Nat. Nanotechnol.* **14**, 658 (2019).
 - [10] S. Li, W. Kang, X. Zhang, T. Nie, Y. Zhou, K. L. Wang, and W. Zhao, *Mater. Horiz.* **8**, 854 (2020).
 - [11] Y. Zhang, Q. Zheng, X. Zhu, Z. Yuan, and K. Xia, *Sci. China: Phys., Mech. Astron.* **63**, 277531 (2020).
 - [12] S. Heinze, K. Von Bergmann, M. Menzel, J. Brede, A. Kubetzka, R. Wiesendanger, G. Bihlmayer, and S. Blügel, *Nat. Phys.* **7**, 713 (2011).
 - [13] N. Romming, A. Kubetzka, C. Hanneken, K. von Bergmann, and R. Wiesendanger, *Phys. Rev. Lett.* **114**, 177203 (2015).
 - [14] H. Yang, A. Thiaville, S. Rohart, A. Fert, and M. Chshiev, *Phys. Rev. Lett.* **115**, 267210 (2015).
 - [15] M. Belmeguenai, J. P. Adam, Y. Roussigné, S. Eimer, T. Devolder, J.-V. Kim, S. M. Cherif, A. Stashkevich, and A. Thiaville, *Phys. Rev. B* **91**, 180405(R) (2015).

- [16] J. Cho, N. H. Kim, S. Lee, J. S. Kim, R. Lavrijsen, A. Solignac, Y. Yin, D. S. Han, N. J. J. Van Hoof, H. J. M. Swagten, B. Koopmans, and C. Y. You, *Nat. Commun.* **6**, 7635 (2015).
- [17] C. Back, V. Cros, H. Ebert, K. Everschor-Sitte, A. Fert, M. Garst, T. Ma, S. Mankovsky, T. L. Monchesky, M. Mostovoy, N. Nagaosa, S. S. P. Parkin, C. Pfleiderer, N. Reyren, A. Rosch, Y. Taguchi, Y. Tokura, K. von Bergmann, and J. Zang, *J. Phys. D: Appl. Phys.* **53**, 363001 (2020).
- [18] A. Soumyanarayanan, M. Raju, A. L. G. Oyarce, A. K. C. Tan, M. Y. Im, A. P. Petrovic, P. Ho, K. H. Khoo, M. Tran, C. K. Gan, F. Ernult, and C. Panagopoulos, *Nat. Mater.* **16**, 898 (2017).
- [19] C. Moreau-Luchaire, C. Moutafis, N. Reyren, J. Sampaio, C. A. F. Vaz, N. Van Horne, K. Bouzheouane, K. Garcia, C. Deranlot, P. Wamnicke, P. Wöhlhüter, J. M. George, M. Weigand, J. Raabe, V. Cros, and A. Fert, *Nat. Nanotechnol.* **11**, 444 (2016).
- [20] L. Wang, C. Liu, N. Mehmood, G. Han, Y. Wang, X. Xu, C. Feng, Z. Hou, Y. Peng, X. Gao, and G. Yu, *ACS Appl. Mater. Interfaces* **11**, 12098 (2019).
- [21] Z. Qin, C. Jin, H. Xie, X. Li, Y. Wang, J. Cao, and Q. Liu, *J. Phys. D: Appl. Phys.* **51**, 425001 (2018).
- [22] Y. Wang, L. Wang, J. Xia, Z. Lai, G. Tian, X. Zhang, Z. Hou, X. Gao, W. Mi, C. Feng, M. Zeng, G. Zhou, G. Yu, G. Wu, Y. Zhou, W. Wang, X. Zhang, and J. Liu, *Nat. Commun.* **11**, 3577 (2020).
- [23] T. Lin, H. Liu, S. Poellath, Y. Zhang, B. Ji, N. Lei, J. J. Yun, L. Xi, D. Z. Yang, T. Xing, Z. L. Wang, L. Sun, Y. Z. Wu, L. F. Yin, W. B. Wang, J. Shen, J. Zweck, C. H. Back, Y. G. Zhang, and W. S. Zhao, *Phys. Rev. B* **98**, 174425 (2018).
- [24] M. Li, D. Lau, M. De Graef, and V. Sokalski, *Phys. Rev. Mater.* **3**, 064409 (2019).
- [25] X. Wang, Y. Wei, K. He, Y. Liu, Y. Huang, Q. Liu, J. Wang, and G. Han, *J. Phys. D: Appl. Phys.* **53**, 215001 (2020).
- [26] L. Fallarino, A. Oelschlägel, J. A. Arregi, A. Bashkatov, F. Samad, B. Böhm, K. Chesnel, and O. Hellwig, *Phys. Rev. B* **99**, 024431 (2019).
- [27] X. Zhang, W. Cai, X. Zhang, Z. Wang, Z. Li, Y. Zhang, K. Cao, N. Lei, W. Kang, Y. Zhang, H. Yu, Y. Zhou, and W. Zhao, *ACS Appl. Mater. Interfaces* **10**, 16887 (2018).
- [28] M. Wang, W. Cai, K. Cao, J. Zhou, J. Wrona, S. Peng, H. Yang, J. Wei, W. Kang, Y. Zhang, J. Langer, B. Ocker, A. Fert, and W. Zhao, *Nat. Commun.* **9**, 671 (2018).
- [29] L. Z. Wang, X. Li, T. Sasaki, K. Wong, G. Q. Yu, S. Z. Peng, C. Zhao, T. Ohkubo, K. Hono, W. S. Zhao, and K. L. Wang, *Sci. China: Phys., Mech. Astron.* **63**, 277512 (2020).
- [30] H. K. Gweon and S. H. Lim, *Jpn. J. Appl. Phys.* **57**, 030301 (2018).
- [31] W. Y. Kim, H. K. Gweon, K. J. Lee, and C. Y. You, *Appl. Phys. Express* **12**, 053007 (2019).
- [32] A. Cao, R. Chen, X. Wang, X. Zhang, S. Lu, S. Yan, B. Koopmans, and W. Zhao, *Nanotechnology* **31**, 155705 (2020).
- [33] X. S. Wang, H. Y. Yuan, and X. R. Wang, *Commun. Phys.* **1**, 31 (2018).
- [34] N. Vidal-Silva, A. Riveros, and J. Escrig, *J. Magn. Magn. Mater.* **443**, 116 (2017).
- [35] A. Cao, X. Zhang, B. Koopmans, S. Peng, Y. Zhang, Z. Wang, S. Yan, H. Yang, and W. Zhao, *Nanoscale* **10**, 12062 (2018).
- [36] A. Lamperti, S. M. Ahn, B. Ocker, R. Mantovan, and D. Ravelosona, *Thin Solid Films* **533**, 79 (2013).
- [37] S. Tacchi, R. E. Troncoso, M. Ahlberg, G. Gubbiotti, M. Madami, J. Åkerman, and P. Landeros, *Phys. Rev. Lett.* **118**, 147201 (2017).
- [38] H. T. Nembach, J. M. Shaw, M. Weiler, E. Jué, and T. J. Silva, *Nat. Phys.* **11**, 825 (2015).
- [39] X. Ma, G. Yu, C. Tang, X. Li, C. He, J. Shi, K. L. Wang, and X. Li, *Phys. Rev. Lett.* **120**, 157204 (2018).
- [40] J.-H. Moon, S.-M. Seo, K.-J. Lee, K.-W. Kim, J. Ryu, H.-W. Lee, R. D. McMichael, and M. D. Stiles, *Phys. Rev. B* **88**, 184404 (2013).
- [41] M. Belmeguenai, Y. Roussigné, S. M. Chérif, A. Stashkevich, T. Petrisor, M. Nasui, and M. S. Gabor, *J. Phys. D: Appl. Phys.* **52**, 125002 (2019).
- [42] See Supplemental Material at <http://link.aps.org/supplemental/10.1103/PhysRevB.104.064421> for the M - H curves and the M_s and t_{DL} fitting for as-deposited and annealed samples (also see Ref. [43]); for MFM images for multirepetition samples; for micromagnetic simulations (also see Ref. [53]); and for BLS measurements in annealed samples.
- [43] H. K. Gweon, S. J. Yun, and S. H. Lim, *Sci. Rep.* **8**, 1266 (2018).
- [44] S. Zhang, J. Zhang, Y. Wen, E. M. Chudnovsky, and X. Zhang, *Commun. Phys.* **1**, 36 (2018).
- [45] S. D. Pollard, J. A. Garlow, J. Yu, Z. Wang, Y. Zhu, and H. Yang, *Nat. Commun.* **8**, 14761 (2017).
- [46] J. Tang, Y. Wu, L. Kong, W. Wang, Y. Chen, Y. Wang, Y. Soh, Y. Xiong, M. Tian, and H. Du, *Natl. Sci. Rev.* **8**, nwa200 (2021).
- [47] A. Casiraghi, H. Corte-León, M. Vafaei, F. Garcia-Sanchez, G. Durin, M. Pasquale, G. Jakob, M. Kläui, and O. Kazakova, *Commun. Phys.* **2**, 145 (2019).
- [48] M. T. Johnson, P. J. H. Bloemen, F. J. A. Den Broeder, and J. J. De Vries, *Rep. Prog. Phys.* **59**, 1409 (1996).
- [49] H. S. Song, K. D. Lee, J. W. Sohn, S. H. Yang, S. S. P. Parkin, C. Y. You, and S. C. Shin, *Appl. Phys. Lett.* **102**, 102401 (2013).
- [50] V. Karakas, A. Gokce, A. T. Habiboglu, S. Arpacı, K. Ozbozduman, I. Cinar, C. Yanik, R. Tomasello, S. Tacchi, G. Siracusano, M. Carpentieri, G. Finocchio, T. Hauet, and O. Ozatay, *Sci. Rep.* **8**, 7180 (2018).
- [51] T. Böttcher, K. Lee, F. Heussner, S. Jaiswal, G. Jakob, M. Kläui, B. Hillebrands, T. Brächer, and P. Pirro, *IEEE Magn. Lett.* **57**, 1600207 (2021).
- [52] J. Mulkers, B. Van Waeyenberge, and M. V. Milošević, *Phys. Rev. B* **95**, 144401 (2017).
- [53] S. Woo, K. Litzius, B. Krüger, M. Y. Im, L. Caretta, K. Richter, M. Mann, A. Krone, R. M. Reeve, M. Weigand, P. Agrawal, I. Lemesch, M. A. Mawass, P. Fischer, M. Kläui, and G. S. D. Beach, *Nat. Mater.* **15**, 501 (2016).
- [54] A. Hrabec, N. A. Porter, A. Wells, M. J. Benitez, G. Burnell, S. McVitie, D. McGrouther, T. A. Moore, and C. H. Marrows, *Phys. Rev. B* **90**, 020402(R) (2014).
- [55] X. Chen, C. Feng, Z. L. Wu, F. Yang, Y. Liu, S. Jiang, M. H. Li, and G. H. Yu, *Appl. Phys. Lett.* **104**, 052413 (2014).